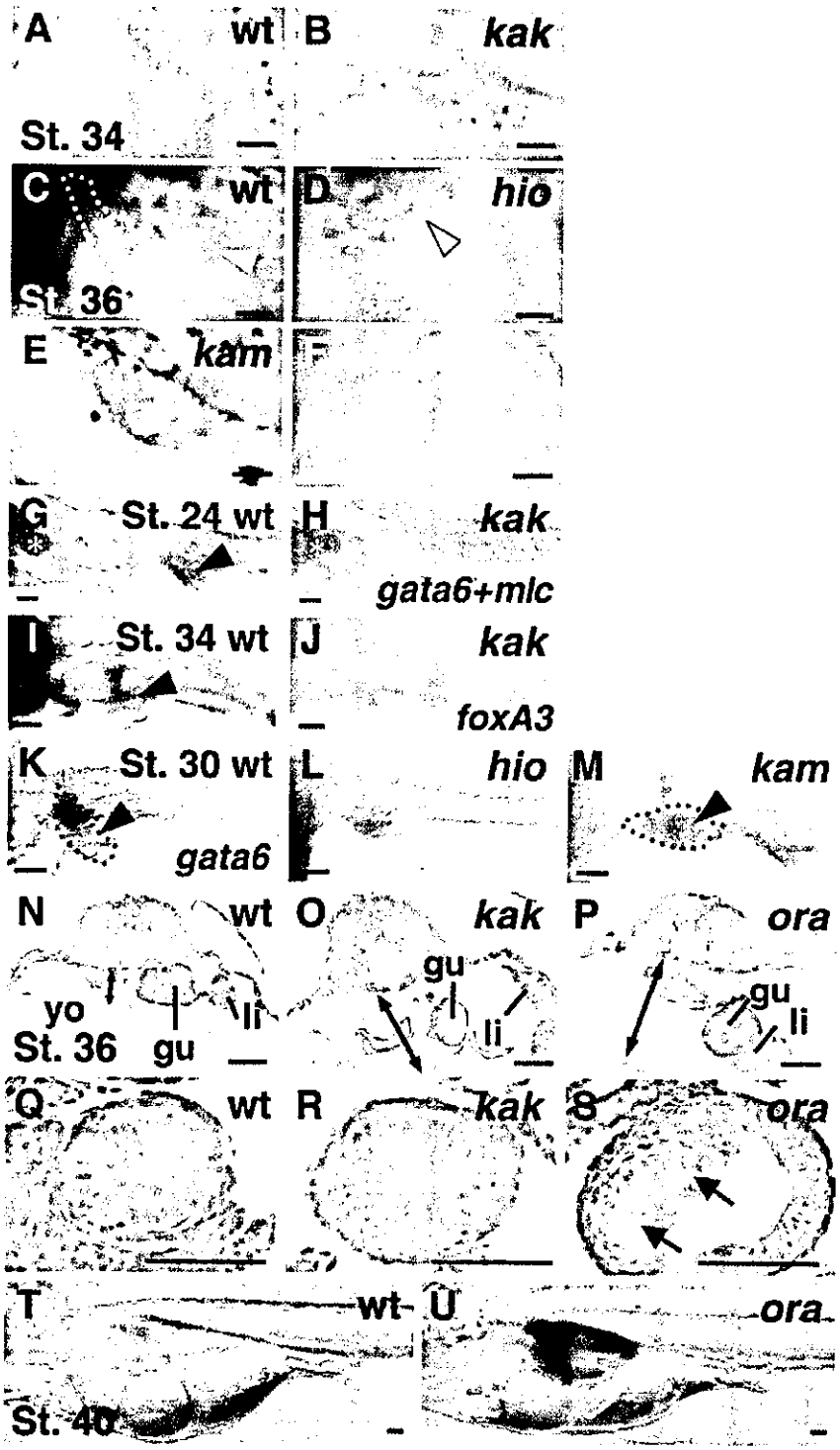

Fig. 2. *kak*, *hio*, *kam* and *ora* mutations affect liver morphogenesis. (A–F, T, and U) Live embryos; (G–M) Fixed embryos stained by in situ hybridization; (N–S) Histological sections stained with hematoxylin and eosin. in situ hybridization was performed using the probes of (G and H) *gata6* and *mlc*; (I and J) *foxA3*; and (K–M) *gata6*. (Q–S) Enlarged view of (N–P), respectively. (A–F, K–M, T and U) Lateral views, (G and H) dorsal views, anterior to the left, (N–S) Cross-sections. (A and B) st. 34; (C–F) st. 36; (G and H) st. 24; (I and J) st. 34; (K–M) st. 30; (N–S) st. 36; (T and U) st. 40. (A, C, G, I, K, N, Q, and T) Wild-type sibling embryos; (B, D, F, H, J, L, M, O, P, R, S, and U) Mutant embryos of (B, H, J, O, and R) *kak*; (D and L) *hio*; (E and M) *kam*; (F, P, S, and U) *ora*. Both arrows indicate the space between the yolk and the embryo proper. White broken lines demarcate the liver. Black and white arrowheads and white asterisks indicate the hepatic bud, gall bladder, and heart, respectively. Black arrows indicate the affected epithelial structure of the gut in the *ora* mutant. Gu: gut, Li: liver, yo: yolk. Scale bars correspond to 50 μm.

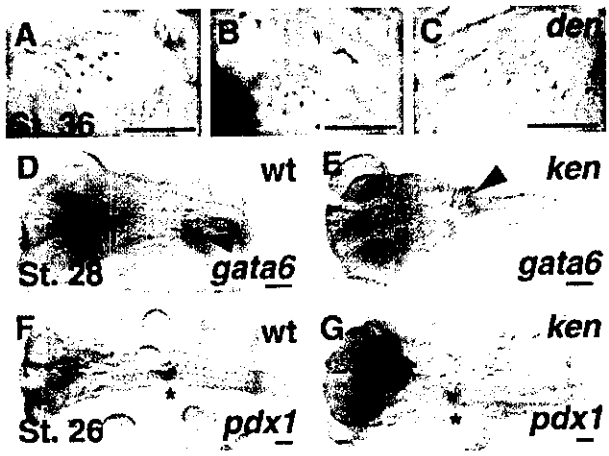

Fig. 3. *ken* and *den* mutations affect liver laterality. (A–C) Live embryos; (D–G) Embryos stained by in situ hybridization using the *gata6* (D and E) and *pdx1* (F and G) probes. (A–C) Lateral views, (D–G) dorsal views, (A, B, D–G) anterior to the left, (C) anterior to the right. (A and D) Wild-type sibling embryos; (B, C, E, and G) Mutant embryos, (B and E) *ken*, (C) *den* mutant embryos. White broken lines demarcate the livers. Black arrowheads, white arrowheads, and black asterisks indicate the liver, gall bladder, and pancreas, respectively. Scale bars correspond to 150 μm.

wild-type embryos, epithelial cells were irregularly arranged in *ora* mutant embryos (arrows in Fig. 2S).

2.2.2. Mutations affecting liver laterality

Mutations in three genes, *kendama* (*ken*), *dendendaiko* (*den*) and *hanetsuki* (*hat*), caused altered liver laterality (Fig. 3). In addition to the liver, the gall bladder, hepatic vein and blood vessels from the liver to the Cuvierian duct were also inverted in these mutant embryos. All mutant embryos hatched and their larvae swam well, suggesting that the altered laterality of the liver and other organs do not affect embryonic viability.

In *ken* mutant embryos, the laterality of the liver and heart was found to be uncoupled, as shown in Table 2. *ken* mutant embryos are classified into four groups according to the location of the liver and heart: (1) the liver shifts to the center and the heart is normally located, L(c)H(n); (2) the liver shifts to the center and the heart was inverted, L(c)H(i); (3) the liver shifts to the right with the heart normally positioned, L(r)H(n); (4) the liver shifts to the right and the heart was inverted, L(r)H(i). These phenotypes were observed in subsequent generations. A *ken* mutant embryo of L(c)H(n) at st. 36 is shown in Fig. 3B. In the embryo in which the liver and gall bladder were located at the center of the body, the liver was not visible from the left view but the heart was observed at the normal location (data not shown). Since, in Medaka the pancreas, detected by the expression of *pdx1*, lies at the center of embryos in the wild-type embryo at st. 26 (Assouline et al., 2001), we could not determine the laterality of the pancreas in *ken* mutant embryos (Fig. 3F,G).

In *den* and *hat* mutant embryos, the liver, gall bladder, and the heart were all inverted in these mutants, as shown in Fig. 3C and Table 2. These results suggest that while *den* and *han* are required for the general laterality of the body, *ken* is required for coupling the laterality of the liver and heart.

2.2.3. Mutations affecting color of bile in the gall bladder

Mutations in three genes, *suou* (*suo*), *akane* (*aka*) and *ominaeshi* (*omi*), affected the color of bile in the gall bladder (Fig. 4). Bile in the wild-type embryo at st. 35 was light green, as shown in Fig. 4A. The bile colors in the three mutants, *suo*, *aka* and *omi*, were orange, deep red and white, respectively (Fig. 4B–D). *aka* and *omi* mutant embryos were embryonic lethal, but *suo* mutant embryos hatched and *suo* homozygotes were fertile.

To determine whether these mutations affect either erythropoiesis or hemoglobin-bile metabolism, we first carried out hemoglobin staining with *o*-dianisidine. As shown in Fig. 4E–H, the blood vessels and heart, but not the gall bladder, were stained in *suo* mutant embryos, but were not stained in *aka* and *omi* mutant embryos. We next examined the expression of *globin* genes by in situ hybridization. Medaka embryos express three types of *globin*, *α-0*, *α-1*, and *β-1* (Maruyama et al., 2002). *α-0*, *α-1*, and *β-1 globins* were expressed in *suo* mutants at st. 33 (Fig. 4I,J,M,N, and data not shown), whereas *α-0*, but not *α-1* and *β-1 globins* were expressed in *aka* mutant embryos (Fig. 4K,O, and data not shown). None of *α-0*, *α-1*, and *β-1 globins* were expressed in *omi* mutant embryos (Fig. 4L,P, and data not shown). These results indicate that *aka* and *omi* mutations affect erythropoiesis. On the other hand,

Table 2
Frequency of alteration of liver and heart laterality

		Laterality phenotype (%)						
		Total	L(l) H(n)	L(l) H(i)	L(c) H(n)	L(c) H(i)	L(r) H(n)	L(r) H(i)
ken	mut	39	0	0	10 (26)	16 (40)	3 (7)	10 (26)
	sib	102	101 (99)	1 (1)	0	0	0	0
hat	mut	21	0	0	0	0	0	21 (100)
	sib	96	95 (99)	1 (1)	0	0	0	0
den	mut	19	0	0	0	0	1 (6)	18 (94)
	sib	120	119 (99)	1 (1)	0	0	0	0

L, liver; H, heart; l, left; c, center; r, right; n, normal; i, invert.

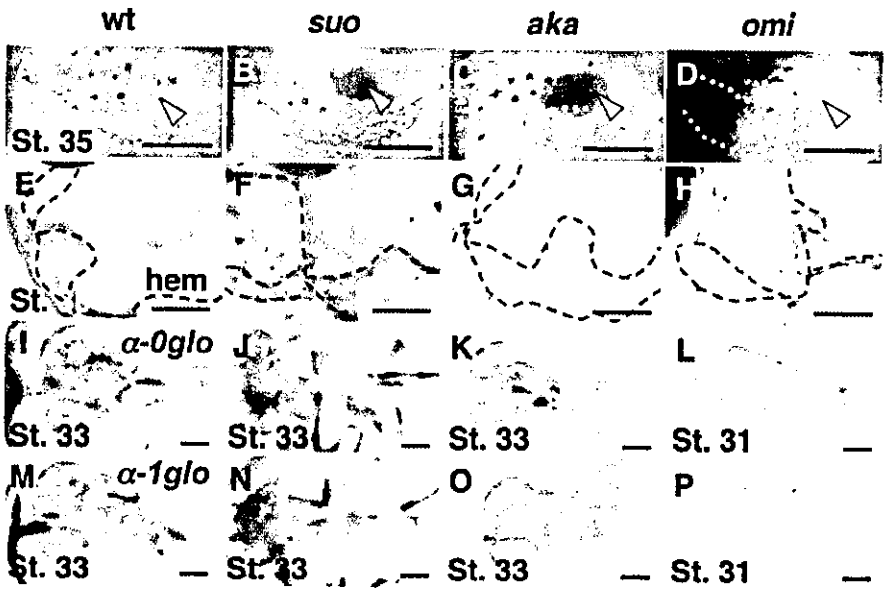

Fig. 4. *aka*, *suo* and *omi* mutations affect bile color. (A–D) Live embryos; (E–H) Hemoglobin staining; (I–P) in situ hybridization, using (I–L) the *α-0 globin*, and (M–P) *α-1 globin* probes. (A–D) st. 35; (E–H) st. 36; (I–K, M–O) st. 33 and (L and P) st. 31. (A, E, I, and M) wild-type sibling embryos, (B, F, J, and N) *suo*, (C, G, K, and O) *aka* and (D, H, L, and P) *omi* mutant embryos. White arrowheads and white broken lines indicate the gall bladder and margin of the liver, respectively. Black broken lines show the Cuvierian duct. Black to brownish spots are melanophores on the yolk. Scale bars correspond to 200 μm.

erythropoiesis appears normal and orange bile in the gall bladder is not due to the accumulation of erythrocytes in *suo* mutant embryos, suggesting that *suo* mutation may affect hemoglobin–bilirubin metabolism.

2.2.4. Mutations affecting lipid metabolism

The fluorescence intensities of PED6 metabolites markedly decreased in three mutant embryos, *ukon* (*uko*), *aonibi* (*aon*) and *uguisucha* (*ugu*), at st. 35 (Fig. 5C–F). To examine whether the decrease in fluorescence intensity is due to the inability of swallowing PED6, we loaded the three mutant embryos with BODIPY-FL-C5, an unquenched form of PED6. All the mutants swallowed the unquenched form of PED6, and the gut, liver and gall bladder showed fluorescence as wild-type embryos (Fig. 5G–J).

uko and *aon* mutant embryos appeared normal in the morphologies of the liver, gall bladder and intestine at st. 35 as shown in Fig. 5B, and *ugu* mutant embryos started to show retardation in development from st. 35 (data not shown). *uko* mutant embryos could hatch but their larvae died a few days after hatching (data not shown). Both *aon* and *ugu* mutant embryos were embryonic lethal. The forebrain was reduced in size from st. 23 in *aon* mutant embryos (Kitagawa et al., 2004). These results suggest that the *uko*, *aon* and *ugu* genes are required for the metabolism or transport of lipids in the hepatobiliary system.

2.2.5. Mutations affecting patterning of endoderm

Six mutations affecting formation of the endodermal rod and/or hepatic bud were identified. Mutations in the *fukuwarai* (*fku*) genes affected endodermal rod morphogenesis (Fig. 6G). Although in *fku* mutant embryos *foxA3* was expressed in the pharynx, hepatic region and the gut (Fig. 6, open circle, arrow head and asterisk, respectively), parts of the endodermal rod were randomly dislocated (Fig. 6G arrow) as other epithelial structures, such as the head structures originated from neuroepithelium (Fig. 6B closed arrow, Kitagawa et al., 2004).

In *sakura* (*sak*) mutant embryos, *foxA3* was expressed in the gut and hepatic region, but not in the pharynx (Fig. 6H). Growth of the hepatic region appeared to be affected and anterior part of the endodermal rod may be missing or misspecified. In *sak* mutant embryos, the heart was not formed and the eyes became degenerated at st. 28 (Fig. 6C, closed arrow).

In embryos with mutations in three genes, *akatsuki* (*aku*), *akebono* (*ake*) and *mochizuki* (*moc*), the endodermal rod was missing (Fig. 6I, data not shown). These mutants exhibited a body patterning phenotypes similar to those of *one-eyed-pinhead* (*oep*) zebrafish mutants (Fig. 6D, data not shown, Kitagawa et al., 2004). While embryos with mutations in only one gene exhibit the *oep* mutant phenotypes, those in three genes display similar phenotypes in both body patterning and endoderm formation.

In *hirame* (*hir*) mutant embryos, *foxA3* expressing endodermal cells did not converge properly, affecting the endermal rod formation (Fig. 6J open arrow). *hir* mutant embryos were flat and tissues such as the lens and heart were mislocated (Fig. 6E, the closed arrow indicates mislocated lens, Kitagawa et al., 2004).

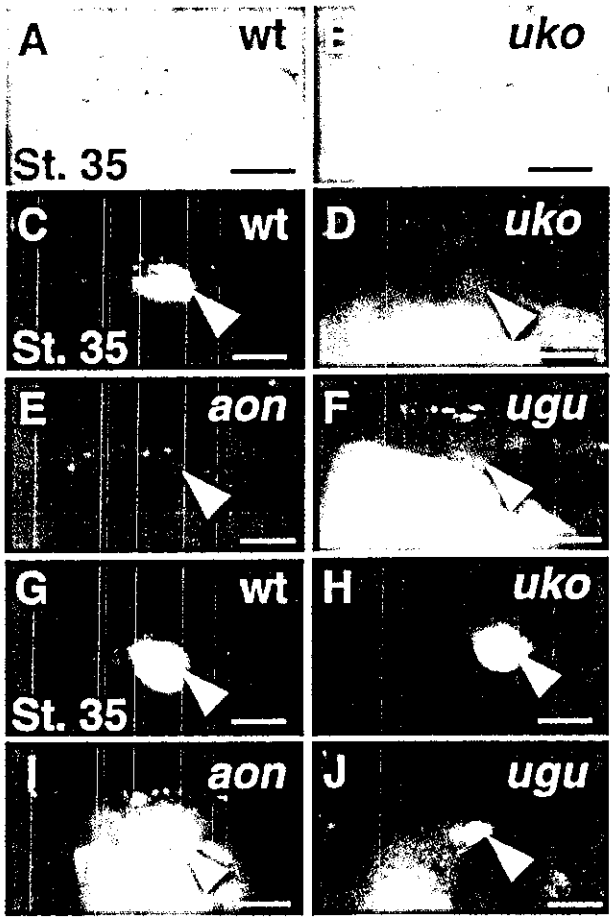

Fig. 5. *uko*, *ugu*, and *aon* mutations affect lipid metabolism. Lateral view, anterior to the left. Live embryos of unstained (A, B), stained with PED6 (C–F) and BODIPY FL-C5 (G–J) at st. 35. (A, C, and G) Wild-type, (B, D, and H) *uko*, (E and I) *aon* and (F and J) *ugu*. Metabolized PED6 (C-F) or BODIPY FL-C5 (G–J) can been seen as a green emission (Em: 505 nm) in the gall bladder (white arrowheads). White broken lines demarcate the margin of the liver. Scale bars correspond to 200 μm.

3. Discussion

3.1. Screening for mutations affecting liver development in Medaka

Partly due to the functional overlap of genes, particularly in vertebrates, mutagenesis screens in a single species are unlikely to be sufficient for identifying all essential genes involved in a particular biological process Therefore, mutagenesis screens and analyses of Medaka mutants complement those in zebrafish, in identifying a wider repertoire of genes by a forward genetic approach in vertebrates.

Our mutagenesis screen in Medaka identified mutations in 19 genes affecting various aspects of the development of the liver and associated tissues. These mutations are classified into five groups: (1) mutations affecting liver morphogenesis; (2) mutations affecting liver laterality; (3) mutations affecting of bile color; (4) mutations affecting lipid metabolism; and (5) mutations affecting endoderm and hepatic bud formation. In zebrafish, a mutagenesis screen using GFP-transgenic fish, whose developing endoderm or organs arising from endoderm are more conspicuous, is underway (D. Y. R. Stainier, personal communication). Thus, mutagenesis screens in both Medaka and zebrafish should be complementary in identifying conserved and divergent mechanisms of liver development.

In our screen, we initially aimed to identify mutations affecting formation and function of the liver specifically. To this end we carried out a screen by multiple criteria to reveal the specificity of the defect. Majority of mutations that we identified were those affecting tissues in addition to the liver during development. From these results, we deduced that mutations affecting the liver specifically may be very limited and that even if defects are not confined to the liver, mutated genes are important for the formation of the liver or physiological functions in which the liver is involved. Thus expression of these genes identified in our screen may not be restricted to the liver but to the tissues, from which the liver originates or those working with the liver to exert its physiological functions.

3.2. Mutations affecting liver morphogenesis

Several explanations may account for the phenotypes of Group 1 mutants with defects in the liver, and gall bladder and gut. First, cell-autonomous defects may affect the regional morphogenesis of the endodermal rod, resulting in altered morphologies of the liver, gall bladder and gut. Second, non-cell-autonomous defects such as the interaction between the surrounding lateral mesoderm and endodermal rod may cause the phenotype. Third, there may be regulatory interactions among the hepatic bud, primordium of the gall bladder and the intestinal bulb. Transplantation experiments to determine the cell autonomy of these mutations would be useful to clarify these possibilities. Finally, since nutrients absorbed from the intestine are metabolized in the liver (Wallace and Pack, 2003; Warga and Stainier, 2002), a defect in the intestine may affect liver growth. The idea that the timing of liver growth is dependent on nourishment from the intestine needs to be further investigated.

In *kak* mutants, although the hepatic bud is formed, the liver is very small at st. 34 and the gall bladder may have shifted its position due to the small liver. This suggests that *kak* is required for the formation of the liver from the hepatic bud.

In *hio* mutants, the liver is small and malformed and the pectoral fin is missing. In zebrafish, some mutations affect the pectoral fin, but no mutations have been reported to affect both the liver and pectoral fin yet (Grandel and Schulte-Merker, 1998; Neumann et al., 1999; van Eeden et al., 1996). It has been suggested that, however, mesodermal components or FGF signaling is

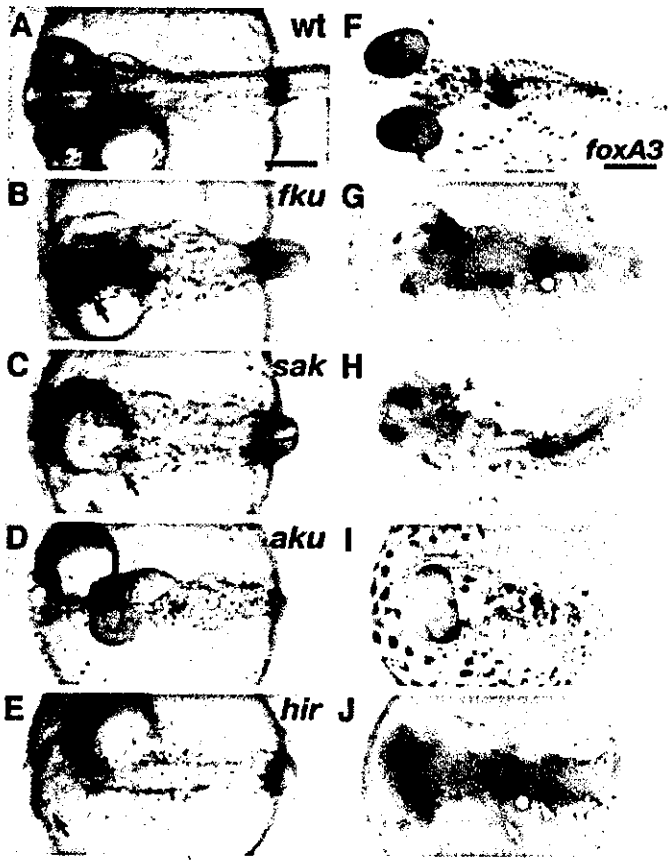

Fig. 6. *fku, sak, aku,* and *hir* mutations affect patterning of endoderm. Dorsal views of (A–E) live embryos and (F–J) embryos stained by in situ hybridization using the *foxA3* probe at st. 28. (A and F) Wild-type embryos, (B and G) *fku*; (C and H) *sak*, (D and I) *aku* and (E and J) *hir* mutant embryos. Open circle, arrowhead, and asterisk indicate the sites where pharynx, hepatic bud, and the gut are normally formed, respectively. Closed arrows show dislocated head structure in B, degenerating eye in C, dislocated lens in E. Open arrows indicate mislocated part of the endodermal rod in G and *foxA3* positive cells inappropriately converged in J. The margin of the embryo was demarcated by the broken line in I. Scale bars correspond to 250 μm.

required for the formation of the pectoral fin and liver (Fischer et al., 2003; Jung et al., 1998; Martin, 1998). It would be interesting to examine mesoderm development and FGF expression in *hio* mutant embryos to further characterize this mutation.

In *kam* mutant embryos, in addition to a malformed liver and gall bladder, the heart is small and blood accumulates near the liver and gut. Such blood accumulation may reflect a defect either in vasculature formation in the liver or in endothelial cell development. In *vegfr2/flk-1* mutant mice with endothelial cell defects, liver budding does not occur. However, in zebrafish, although *cloche* zebrafish mutants lacking all endothelial cells, normal liver budding and development occurs (Field et al., 2003; Stainier et al., 1995). However, severe cardiac edema did not allow analysis of the requirement of endothelial cells during the growth of the liver in those studies. In *kam* mutants, liver budding seems to occur normally, but the growth of the liver may be affected. Detailed analysis of *kam* mutants at the budding and growth periods using endothelial markers would be useful for the further characterization of this mutation.

3.3. Laterality of the liver and other organs

The laterality of all the organs is inverted in most of mutants of zebrafish and mice (Essner et al., 2000; Faucourt et al., 2001; Mochizuki et al., 2002; Schilling et al., 1999), but there are a few reports on uncoupled laterality of the organs (Bisgrove et al., 2000; Field et al., 2003). In zebrafish *flh* and *boz* mutants, the laterality of the liver and heart is randomized and uncoupled (Chin et al., 2000). *flh* is required for specification of the chordamesoderm and *boz* is required for dorsal axis formation. Both *flh* and *boz* are required for early specification of the notochord. Collectively, *ken* mutants show a defect in the laterality of the viscera as observed in *flh* and *boz* mutants but do not show other morphological deficits. An interesting possibility is that *ken* might be a component of the signaling downstream of *boz* and *flh*.

3.4. Mutations affecting bile color

Since a compromised function of the liver readily results in jaundice in human, hemoglobin metabolism producing bilirubin is one of the most important functions of the liver

Hereditary diseases affecting bilirubin metabolism are known in human (Nowicki and Poley, 1998).

Mutations affecting the color of bile in the gall bladder and red blood cells were identified in zebrafish (Ransom et al., 1996; Shafizadeh et al., 2002; Thisse and Zon, 2002; Weistein et al., 1996). *aka* and *omi* mutations also affect erythropoiesis in Medaka. In contrast, *suo* mutation seems to be the first mutation affecting hemoglobin–bilirubin metabolism in zebrafish and Medaka. It would be of interest if *suo* mutation models a human disease.

3.5. Lipid metabolism

PED6 is a substrate for PLA_2 cleavage and a sensitive reporter of its enzymatic activity in vivo (Farber et al., 2001). PLA_2 is important in the generation of lipid signaling molecules, host defenses, lipid absorption and cancer. It is thus a good chemical reagent for screening mutations affecting lipid metabolism. Using PED6, four mutations affecting digestive organ morphology and one mutation affecting bile synthesis or secretion were identified in zebrafish (Farber et al., 2001).

The *uko*, *aon*, and *ugu* mutations may affect steps in the lipid metabolism pathway, such as ingestion and cleavage of the lipid within the intestine, and subsequent hepatobiliary transport to the gall bladder (Faber et al., 2001). Further biochemical characterization is necessary to determine which component of lipid metabolism is affected in Group 4 mutants.

3.6. Mutations affecting endoderm formation and patterning

The phenotypes of *aku*, *ake* and *moc* mutants in patterning of the body, endoderm and mesoderm, are similar to those of zebrafish *oep* mutants with defects in the Nodal signaling pathway (Schier et al., 1996, 1997; Zhang et al., 1998). Zebrafish mutations in other components of the Nodal signaling pathway, such as *cyclops*, *squint* and *smalspur*, exhibit phenotypes substantially different from that of *oep* mutation (Brand et al., 1996). Cloning of three genes, *aku*, *ake* and *moc* genes will clarify the conserved or divergent functions of these genes in endoderm specification.

The *fku* and *hir* mutants show unique phenotypes in the patterning of the body, not recorded yet in the collection of zebrafish mutants. In *fku* mutants, parts of the head, such as the eyes and nose, are mislocated. In *hir* mutants, the body becomes thinner and several tissues, such as the lens and heart, are mislocated. Although the endodermal cells expressing *foxA3* are present, morphogenesis of the hepatic bud and convergence of the endodermal cells did not occur properly in *fku* and *hir* mutants, respectively. Interestingly, the common feature between *fku* and *hir* mutants is the marked defect of cell alignment in the epithelium (Furutani-Seiki et al., unpublished results). Further analysis of *fku* and *hir* mutants using early hepatocyte markers may help clarify the relationship between endodermal epithelialization and morphogenesis or specification of the endodermal rod.

In *sak* mutants, the heart primordium and the anterior part of the endodermal rod are not formed. It has been reported that the cardiac mesoderm is necessary for the induction of hepatic bud in mice (Duncan, 2003; Jung et al., 1999; Rossi et al., 2001). Further investigation of the requirement of *sak* in the heart or liver by transplantation experiments may provide insights into tissue interactions in heart and liver development.

4. Experimental procedures

4.1. Maintenance of fish stocks

Fish maintenance and mating were carried out as described elsewhere (Furutani-Seiki et al., 2004). Briefly, the Kyoto-Cab sub-strain and Kaga strain were used to induce mutations in the male germline by treatment with ENU (Ethyl-Nitroso-Urea). F3 progenies homozygous for induced mutations were generated by a three generation incrossing scheme.

4.2. Screening procedures

Live F3 progenies were screened for developmental defects at st. 32 and 36 using a Leica MZ12.5 dissecting microscope. For functional screening, we used PED6, a fluorescent PLA_2-substrate dye. PLA_2 cleavage liberates the BODIPY-acyl chain of PED6, resulting in unquenching and green fluorescent emission as described previously (Farber et al., 2001). As the control, BODIPY FL-C5, an unquenched form of PED6 was used. Embryos at st. 35 were placed in 0.5 ml of 1 × Balanced Salt Solution (BSS; 110 mM NaCl, 5 mM KCl, 1 mM $CaCl_2$, and 2.2 mM $MgSO_4$, pH 7.2), containing 0.3 μg/ml PED6 or 0.2 μg/ml BODIPY-FL-C5, and incubated in the dark for 4 h at 28 °C. The embryos were then rinsed with 1 × BSS and placed in a glass depression slide. Using a Zeiss Axioplan 2 microscope, samples were examined for fluorescence from PED6 or BODIPY-FL-C5.

4.3. Histological sections

Embryos were dechorionated and fixed in 4% paraformaldehyde in PBS(−) overnight at 4 °C. The embryos were dehydrated with ethanol and stored at −20 °C. For sectioning, they were incubated in xylene and embedded in paraffin at 67 °C. Paraffin embedded embryos were sectioned (4 μm thickness) and stained with hematoxylin and eosin.

4.4. In situ hybridization

Whole mount in situ hybridization was performed as described elsewhere (Sasado et al., 2004), using an

anti-sense DIG-labeled riboprobe generated from Medaka *foxA3*, *gata6*, *mlc*, *pdx1*, *α-0*, *α-1*, and *β-1 globin* cDNA. Dechorionated embryos were fixed with 4% paraformaldehyde and 0.1% Tween 20 in PBS(−). Embryos later than st. 30 were treated with proteinase K and to remove pigmentation, with H_2O_2. Embryos were photographed using a Leica dissecting microscope.

4.5. Whole embryo staining for hemoglobin expression

Hemoglobin staining was done as described previously (Cocca et al., 1995). Dechorionated embryos were stained for 15 min in the dark in *o*-dianisidine (0.6 mg/ml), 0.01 M sodium acetate (pH 4.5), 0.65% H_2O_2 and 40% (vol/vol) ethanol. Stained embryos were cleared with benzyl benzoate/benzyl alcohol (2:1, vol/vol) and examined with a dissecting microscope.

Acknowledgements

We are grateful to Drs Takashi Sasaki and Noboru Nakajima for cloning *gata6* and *foxA3* probes, Dr Raphael Scharfmann for the *pdx1* probe and to Haruka Momose and Takahiro Negishi for in situ hybridization and graphical works. We would like to thank Drs Shuji Terai and Kiwamu Okita for continual discussion and encouragement. This work was supported by the ERATO project of the Japan Science and Technology Agency to H.K.

References

Alexander, J., Stainier, D.Y., 1999. A molecular pathway leading to endoderm formation in zebrafish. Curr. Biol. 9, 1147–1157.

Assouline, S., Nir, S., Lahav, N., 2001. Simulation of non-enzymatic template-directed synthesis of oligonucleotides and peptides. J. Theor. Biol. 208, 117–125.

Bisgrove, B.W., Essner, J.J., Yost, H.J., 2000. Multiple pathways in the midline regulate concordant brain, heart and gut left-right asymmetry. Development 127, 3567–3579.

Brand, M., Heisenberg, C.P., Warga, R.M., Pelegri, F., Karlstrom, R.O., Beuchle, D., Picker, A., Jiang, Y.J., Furutani-Seiki, M., van Eeden, F.J., Granato, M., Haffter, P., Hammerschmidt, M., Kane, D.A., Kelsh, R.N., Mullins, M.C., Odenthal, J., Nusslein-Volhard, C., 1996. Mutations affecting development of the midline and general body shape during zebrafish embryogenesis. Development 123, 129–142.

Chen, J.N., Haffter, P., Odenthal, J., Vogelsang, E., Brand, M., van Eeden, F.J., Furutani-Seiki, M., Granato, M., Hammerschmidt, M., Heisenberg, C.P., Jiang, Y.J., Kane, D.A., Kelsh, R.N., Mullins, M.C., Nusslein-Volhard, C., 1996. Mutations affecting the cardiovascular system and other internal organs in zebrafish. Development 123, 293–302.

Chin, A.J., Tsang, M., Weinberg, E.S., 2000. Heart and gut chiralities are controlled independently from initial heart position in the developing zebrafish. Dev. Biol. 227, 403–421.

Cocca, E., Ratnayake-Lecamwasam, M., Parker, S.K., Camardella, L., Ciaramella, M., di Prisco, G., Detrich, H.W., 1995. Genomic remnants of alpha-globin genes in the hemoglobinless antarctic icefishes. Proc. Natl Acad. Sci. USA 92, 1817–1821.

Douarin, N.M., 1975. An experimental analysis of liver development. Med. Biol. 53, 427–455.

Duncan, S.A., 2003. Mechanisms controlling early development of the liver. Mech. Dev. 120, 19–33.

Essner, J.J., Branford, W.W., Zhang, J., Yost, H.J., 2000. Mesendoderm and left-right brain, heart and gut development are differentially regulated by pitx2 isoforms. Development 127, 1081–1093.

Farber, S.A., Pack, M., Ho, S.Y., Johnson, I.D., Wagner, D.S., Dosch, R., Mullins, M.C., Hendrickson, H.S., Hendrickson, E.K., Halpern, M.E., 2001. Genetic analysis of digestive physiology using fluorescent phospholipid reporters. Science 292, 1385–1388.

Faucourt, M., Houliston, E., Besnardeau, L., Kimelman, D., Lepage, T., 2001. The pitx2 homeobox protein is required early for endoderm formation and nodal signaling. Dev. Biol. 229, 287–306.

Field, H.A., Ober, E.A., Roeser, T., Stainier, D.Y., 2003. Formation of the digestive system in zebrafish. I. Liver morphogenesis. Dev. Biol. 253, 279–290.

Fischer, S., Draper, B.W., Neumann, C.J., 2003. The zebrafish fgf24 mutant identifies an additional level of Fgf signaling involved in vertebrate forelimb initiation. Development 130, 3515–3524.

Furutani-Seiki, M., Sasado, T., Morinaga, C., Suwa, H., Niwa, K., Yoda, H., et al., 2004. A systematic genome-wide screen for mutations affecting organogenesis in Medaka, *Oryzias latipes*. Mech. Dev. 121, 647–658.

Grandel, H., Schulte-Merker, S., 1998. The development of the paired fins in the zebrafish (Danio rerio). Mech. Dev. 79, 99–120.

Grapin-Botton, A., Melton, D.A., 2000. Endoderm development: from patterning to organogenesis. Trends Genet. 16, 124–130.

Jung, J., Zheng, M., Goldfarb, M., Zaret, K.S., 1999. Initiation of mammalian liver development from endoderm by fibroblast growth factors. Science 284, 1998–2003.

Kitagawa, D., Watanabe, T., Saito, K., Asaka, S., Sasado, T., Morinaga, C., et al., 2004. Genetic dissection of the formation of the forebrain in Medaka, *Oryzias latipes*. Mech. Dev. 121, 673–685.

Martin, G.R., 1998. The roles of FGFs in the early developments of vertebrate limbs. Genes Dev. 12, 1571–1586.

Maruyama, K., Yasumasu, S., Iuchi, I., 2002. Characterization and expression of embryonic and adult globins of the teleost *Oryzias latipes* (medaka). J. Biochem. 132, 581–589.

Matsumoto, K., Toshitomi, H., Rossant, J., Zaret, K.S., 2001. Liver organogenesis promoted by endothelial cells prior to vascular function. Science 294, 559–563.

Mochizuki, T., Tsuchiya, K., Yokoyama, T., 2002. Molecular cloning of a gene for inversion of embryo turning (inv) with cystic kidney. Nephrol. Dial. Transplant 17(Suppl. 9), 68–70.

Neumann, C.J., Grandel, H., Gaffield, W., Schulte-Merker, S., Nusslein-Volhard, C., 1999. Transient establishment of anteroposterior polarity in the zebrafish pectoral fin bud in the absence of sonic hedgehog activity. Development 126, 4817–4826.

Nishina, H., Vaz, C., Billia, P., Nghiem, M., Sasaki, T., De la Pompa, J.L., Furlonger, K., Paige, C., Hui, C., Fischer, K.D., Kishimoto, H., Iwatsubo, T., Katada, T., Woodgett, J.R., Penninger, J.M., 1999. Defective liver formation and liver cell apoptosis in mice lacking the stress signaling kinase SEK1/MKK4. Development 126, 505–516.

Nowicki, M.J., Poley, J.R., 1998. The hereditary hyperbilirubinaemias. Baillieres Clin. Gastroenterol. 12, 355–367.

Ober, E.A., Field, H.A., Stainier, D.Y., 2003. From endoderm formation to liver and pancreas development in zebrafish. Mech. Dev. 120, 5–18.

Pack, M., Solnica-Krezel, L., Malicki, J., Neuhauss, S.C., Schier, A.F., Stemple, D.L., Driever, W., Fishman, M.C., 1996. Mutations affecting development of zebrafish digestive organs. Development 123, 321–328.

Ransom, D.G., Haffter, P., Odenthal, J., Brownlie, A., Vogelsang, E., Kelsh, R.N., Brand, M., van Eeden, F.J., Furutani-Seiki, M., Granato, M., Hammerschmidt, M., Heisenberg, C.P., Jiang, Y.J., Kane, D.A., Mullins, M.C., Nusslein-Volhard, C., 1996. Characterization of zebrafish mutants with defects in embryonic hematopoiesis. Development 123, 311–319.

Rossi, J.M., Dunn, N.R., Hogan, B.L., Zaret, K.S., 2001. Distinct mesodermal signals, including BMPs from the septum transversum

mesenchyme, are required in combination for hepatogenesis from the endoderm. Genes Dev. 15, 1998–2009.
Sasado, T., Morinaga, C., Niwa, K., Shinomiya, A., Yasuoka, A., Suwa, H., et al., 2004. Mutations affecting early distribution of primordial germ cells in Medaka (*Oryzias latipes*) embryo. Mech. Dev. 121, 817–828.
Schier, A.F., Neuhauss, S.C., Harvey, M., Malicki, J., Solnica-Krezel, L., Stainier, D.Y., Zwartkruis, F., Abdelilah, S., Stemple, D.L., Rangini, Z., Yang, H., Driever, W., 1996. Mutations affecting the development of the embryonic zebrafish brain. Development 123, 165–178.
Schier, A.F., Neuhauss, S.C., Helde, K.A., Talbot, W.S., Driever, W., 1997. The one-eyed pinhead gene functions in mesoderm and endoderm formation in zebrafish and interacts with no tail. Development 124, 327–342.
Schilling, T.F., Concordet, J.P., Ingham, P.W., 1999. Regulation of left-right asymmetries in the zebrafish by Shh and BMP4. Dev. Biol. 210, 277–287.
Shafizadeh, E., Paw, B.H., Foott, H., Liao, E.C., Barut, B.A., Cope, J.J., Zon, L.I., Lin, S., 2002. Characterization of zebrafish merlot/chablis as non-mammalian vertebrate models for severe congenital anemia due to protein 4.1 deficiency. Development 129, 4359–4370.
Stainier, D.Y., Weinstein, B.M., Detrich, H.W. 3rd, Zon, L.I., Fishman, M.C., 1995. Cloche, an early acting zebrafish gene, is required by both the endothelial and hematopoietic lineages. Development 121, 3141–3150.
Tam, P.P., Kanai-Azuma, M., Kanai, Y., 2003. Early endoderm development in vertebrates: lineage differentiation and morphogenetic function. Curr. Opin. Genet. Dev. 13, 393–400.
Thisse, C., Zon, L., 2002. Organogenesis-heart and blood formation from the zebrafish point of view. Science 295, 457–462.
van Eeden, F.J., Granato, M., Schach, U., Brand, M., Furutani-Seiki, M., Haffter, P., Hammerschmidt, M., Heisenberg, C.P., Jiang, Y.J., Kane, D.A., Kelsh, R.N., Mullins, M.C., Odenthal, J., Warga, R.M., Nusslein-Volhard, C., 1996. Genetic analysis of fin formation in the zebrafish. Danio rerio. Development 123, 255–262.
Wada, T., Joza, N., Cheng, H.M., sasaki, T., Kozieradzki, I., Bachmaier, K., Katada, T., Schreiber, M., Wagner, E.F., Nishina, H., Penninger, J.M., 2004. MKK7 couples stress signaling to G2/M cell cycle progression and cellular senescence. Nat. Cell Biol. 6, 215–226.
Wallace, K.N., Pack, M., 2003. Unique and conserved aspects of gut development in zebrafish. Dev. Biol. 255, 12–29.
Warga, R.M., Stainier, D.Y., 2002. The guts of endoderm formation. Results Probl. Cell Differ. 40, 28–47.
Watanabe, T., Nakagawa, K., Ohata, S., Kitagawa, D., Nishitai, G., Seo, J., Tanemura, S., Shimizu, N., Kishimoto, H., Wada, T., Aoki, J., Arai, H., Iwatsubo, T., Mochita, M., Satake, M., Ito, Y., Matsuyama, T., Mak, T.W., Penninger, J.M., Nishina, H., Katada, T., 2002. SEK1/MKK4-mediated SAPK/JNK signaling participates in embryonic hepatoblast proliferation via a pathway different from NF-κB-induced anti-apoptosis. Dev. Biol. 250, 332–347.
Weistein, B., Schier, A., Abdelilar, S., Malicki, J., Solnica-Krezel, L., Stemple, D., Stainier, D.Y., Zwartkruis, F., Driever, W., Fishman, M., 1996. Hematopoietic mutations in the zebrafish. Development 123, 303–309.
Zaret, K.S., 2001. Hepatocyte differentiation: from the endoderm and beyond. Curr. Opin. Genet. Dev. 11, 568–574.
Zaret, K.S., 2002. Regulatory phases of early liver development: paradigms of organogenesis. Nat. Rev. Genet. 3, 499–512.
Zhang, J., Talbot, W.S., Schier, A.F., 1998. Positional cloning identifies zebrafish one-eyed pinhead as a permissive EGF-related ligand required during gastrulation. Cell 92, 241–251.

Glossary

hiohgi:	a traditional Japanese hand fan for court functions;
kakurembo:	a game of hide-and-seek;
kamifusen:	a balloon made of paper;
origami:	art of folding paper;
kendama:	Japanese toy with a wooden cup and a ball on a thread, where one tries to catch the ball in the cup;
hanetsuki:	traditional Japanese badminton using colored wooden racquets and a shuttlecock;
dendendaiko:	a Japanse drum for children that makes a sound by turning it upside down;
akane, suou:	traditional Japanese term for red;
ominaeshi:	a traditional Japanese term for white;
uguisucha, ukon:	traditional Japanese dark yellow color;
aonibi:	dark green;
fukuwarai:	Japanese jigsaw-puzzle to make with face blindfolded;
sakura:	cherry blossom;
akebono:	rising sun;
akatsuki, mochizuki:	full moon;
hirame:	flounder

Available online at www.sciencedirect.com
SCIENCE DIRECT
Toxicology Letters 152 (2004) 175–181
Toxicology Letters
www.elsevier.com/locate/toxlet

Requirement of MKK4 and MKK7 for $CdCl_2$- or $HgCl_2$-induced activation of c-Jun NH_2-terminal kinase in mouse embryonic stem cells

Masato Matsuoka [a,b,*], Hideki Igisu [b], Kentaro Nakagawa [c], Toshiaki Katada [c], Hiroshi Nishina [c]

[a] *Department of Hygiene and Public Health (1), School of Medicine, Tokyo Women's Medical University, 8-1 Kawada-cho, Shinjuku-ku, Tokyo 162-8666, Japan*
[b] *Department of Environmental Toxicology, Institute of Industrial Ecological Sciences, University of Occupational and Environmental Health, 1-1 Iseigaoka, Yahatanishi-ku, Kitakyushu 807-8555, Japan*
[c] *Department of Physiological Chemistry, Graduate School of Pharmaceutical Sciences, University of Tokyo, 7-3-1 Hongo, Bunkyo-ku, Tokyo 113-0033, Japan*

Received 10 March 2004; received in revised form 27 April 2004; accepted 28 April 2004

Available online 15 June 2004

Abstract

c-Jun NH_2-terminal kinase (JNK), also known as stress-activated protein kinase (SAPK), is activated primarily by inflammatory cytokines and environmental stresses including toxic metal exposure. To reveal the upstream kinase responsible for JNK activation by toxic metals, the phosphorylation status and the activity of JNK were examined in mouse embryonic stem (ES) cells lacking MKK4 or MKK7 following exposure to $CdCl_2$ or $HgCl_2$. Treatment with $CdCl_2$ or $HgCl_2$ induced the phosphorylation of JNK in a dose- and time-dependent manner in wild-type ES cells. In both *mkk4*$^{-/-}$ and *mkk7*$^{-/-}$ ES cells, $CdCl_2$- or $HgCl_2$-induced phosphorylation and activation of JNK were suppressed significantly. However, in *mkk7*$^{-/-}$ ES cells treated with $CdCl_2$ and $HgCl_2$, JNK activation was not abolished (suppressed by 56% and 78%, respectively). These findings suggest that the full activation of JNK by toxic metal exposure requires both MKK4 and MKK7, and these upstream kinases might contribute differentially in JNK activation between mouse ES cells exposed to $CdCl_2$ and $HgCl_2$.

Keywords: c-Jun NH_2-terminal kinase; MKK4; MKK7; $CdCl_2$; $HgCl_2$; ES cells

1. Introduction

Mitogen-activated protein kinases (MAPKs) are a family of Ser/Thr protein kinases that transmit signals into the nucleus, and have been shown to participate in a diverse array of cellular functions such as the control of gene expression, cell proliferation, differentiation, development, inflammatory response, and

Abbreviations: JNK, c-Jun NH_2-terminal kinase; SAPK, stress-activated protein kinase; ES, embryonic stem; MAPK, mitogen-activated protein kinase; ERK, extracellular signal-regulated protein kinase

* Corresponding author. Tel.: +81-3-3353-8111; fax: +81-3-5269-7419.
E-mail address: matsuoka@research.twmu.ac.jp (M. Matsuoka).

0378-4274/$ – see front matter © 2004 Elsevier Ireland Ltd. All rights reserved.
doi:10.1016/j.toxlet.2004.04.033

apoptosis in mammalian systems (Chang and Karin, 2001; Weston and Davis, 2002). c-Jun NH_2-terminal kinase (JNK), also known as stress-activated protein kinase (SAPK), represents one subgroup of MAPKs that is activated primarily by inflammatory cytokines and environmental stresses such as ultraviolet radiation, ionizing radiation, heat shock, osmotic shock, protein synthesis inhibitor, and chemical mutagens (Kyriakis and Avruch, 1996; Robinson and Cobb, 1997). In addition, we have found that environmentally contaminating toxic metals such as cadmium (Matsuoka and Igisu, 1998), inorganic mercury (Matsuoka et al., 2000), and tributyltin (Yu et al., 2000) activate JNK pathway. However, functions and molecular mechanisms of toxic metal-induced JNK activation have not yet been known.

For the activation, JNK requires the dual phosphorylation of Thr and Tyr residues located in a Thr-Pro-Tyr motif between kinase subdomains VII and VIII (Cobb and Goldsmith, 1995). This phosphorylation is catalyzed by the dual specific kinases MKK4 (also known as SEK1 or MEK4) and MKK7 (SEK2), while MKK4 has a preference for the Tyr residue and MKK7 for the Thr residue (Weston and Davis, 2002). In vitro, JNK is activated synergistically by these two upstream kinases (Lawler et al., 1998). With respect to cadmium, it has been reported that JNK activation was suppressed partially by expression of dominant negative mutant of MKK7, but not that of MKK4 in human non-small-cell lung carcinoma cells (Chuang and Yang, 2001; Chuang et al., 2000) and rat mesangial cells (Ding and Templeton, 2000). These findings suggest that cadmium might activate JNK through MKK7, but not MKK4 in vivo. On the other hand, the activation of JNK by ultraviolet, heat shock, sorbitol-induced osmolarity change, or the protein synthesis inhibitor anisomycin was markedly attenuated in mouse embryonic stem (ES) cells targeting either the *mkk4* or the *mkk7* gene (Kishimoto et al., 2003), indicating that both MKK4 and MKK7 are required for the activation of JNK by these stimuli in mouse ES cells. To clarify whether signaling pathway leading to JNK activation by toxic metals is distinct from the case of other cellular stresses, the phosphorylation status and the activity of JNK were examined in $mkk4^{-/-}$ and $mkk7^{-/-}$ ES cells following exposure to $CdCl_2$ or $HgCl_2$. The application of these ES cells lacking either MKK4 or MKK7 would be more beneficial than other cells expressed with dominant negative form of them.

2. Materials and methods

2.1. Cell culture and treatments

The murine ES cell line E14K (wild-type), $mkk4^{-/-}$ mutant cell line made by the *mkk4* gene targeting (Nishina et al., 1997), and $mkk7^{-/-}$ mutant cell line made by the *mkk7* gene targeting (Kishimoto et al., 2003) were maintained in Dulbecco's modified Eagle's medium supplemented with 15% fetal calf serum (GIBCO, Invitrogen Corp., Carlsband, CA, USA) and leukemia inhibitory factor as described previously (Kishimoto et al., 2003). Wild-type, $mkk4^{-/-}$ and $mkk7^{-/-}$ ES cells (passage number 10–15) were plated at 5×10^5 cells per well (for Western immunoblotting) or 1.6×10^6 cells per well (for JNK activity assay) in six-well culture plates coated with 1% gelatin, and cultured for overnight. Then, medium was changed to serum-free medium containing $CdCl_2$ (Sigma Chemical Co., St. Louis, MO, USA) or $HgCl_2$ (Nacalai Tesque, Osaka, Japan). Untreated control cells were incubated with serum-free medium, and were treated identically to cells incubated with $CdCl_2$ or $HgCl_2$. Initially, dose (1 μM, 5 μM, 10 μM, 20 μM, or 40 μM) and time (5 min, 15 min, 30 min, 45 min, or 60 min) of $CdCl_2$ or $HgCl_2$ exposure for the sufficient induction of JNK phosphorylation were determined in wild-type ES cells. Based on these experiments, each ES cell line was incubated with 20 μM of $CdCl_2$ or $HgCl_2$ for 1 h. All experiments were repeated three (for Western immunoblotting) or four times (for JNK activity assay). Data were all obtained from two independently derived ES cell clones with comparable results.

2.2. Western immunoblotting

After the incubation with $CdCl_2$ or $HgCl_2$, ES cells were washed with phosphate-buffered saline, and lysed with sodium dodecyl sulfate (SDS)-polyacrylamide gel Laemmli sample buffer. Cell lysates were collected, sonicated, and boiled for 5 min. Twenty micrograms of protein was subjected to SDS-polyacrylamide gel electrophoresis on a 10%

polyacrylamide gel and transferred to a nitrocellulose membrane (Hybond-ECL, Amersham Pharmacia Biotech, Buckinghamshire, England). The membrane was blocked with 5% non-fat milk or bovine serum albumin in Tris-buffered saline containing 0.1% Tween 20 for 1 h at room temperature. The membrane was incubated overnight at 4 °C with the primary antibody diluted 1:1000. The antibodies used were phospho-SAPK/JNK (Thr^{183}/Tyr^{185}) antibody, phosphorylation state-independent SAPK/JNK antibody, phospho-p38 MAPK (Thr^{180}/Tyr^{182}) antibody, phosphorylation state-independent p38 MAPK antibody, phospho-p44/42 MAPK (Thr^{202}/Tyr^{204}) antibody, phosphorylation state-independent p44/42 MAPK antibody, phospho-specific c-Jun (Ser^{63}) antibody (Cell Signaling Technology, Inc., Beverly, MA, USA), anti-ACTIVE JNK antibody (Promega Corporation, Madison, IL, USA), MEK-4 (C-20) antibody (Santa Cruz Biotechnology Inc., Santa Cruz, CA, USA), and rat monoclonal antibody against MKK7 (KN-004) prepared by Kishimoto et al. (2003). Protein was detected with a Phototope-HRP Western blot detection kit (Cell Signaling Technology). For the detection of MKK7 protein, a SuperSignal West Femto Maximum Sensitivity Substrate (Pierce Chemical Co., Rockford, IL, USA) was used. After the immunodetection, some blots were incubated with a Restore Western Blot Stripping Buffer (Pierce) for 30 min at room temperature, and reprobed with each phosphorylation state-independent MAPK antibody. The bands on the developed films were quantified with NIH Image Version 1.63.

2.3. JNK activity assay

The in vitro activity of JNK was measured using a SAPK/JNK assay kit (Cell Signaling Technology) according to the instruction from the manufacturer. Briefly, cell lysates were incubated with GST-c-Jun (1–89) fusion protein overnight, and the precipitated JNK was subjected to in vitro kinase assay using GST-c-Jun (1–89) as substrate. Phosphorylation of GST-c-Jun on Ser^{63} was analyzed with immunoblotting using phospho-c-Jun antibody. The bands on the developed films were quantified with NIH Image Version 1.63.

2.4. Statistical analysis

Results were expressed as mean ± S.D. The statistical significance was determined by one-way analysis of variance followed by the Dunnett multiple comparison test. $P < 0.05$ was considered as statistically significant.

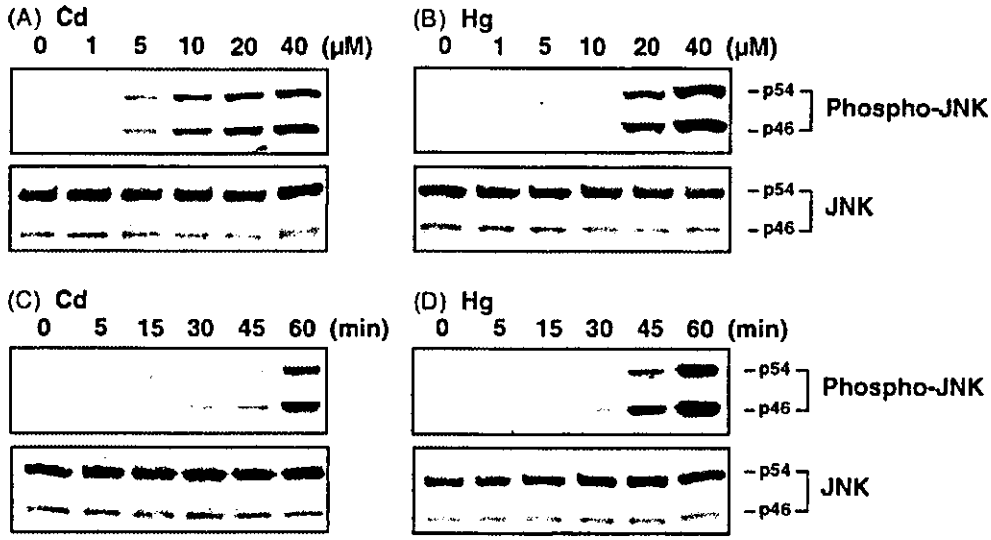

Fig. 1. Dose effects (A, B) and time course (C, D) of $CdCl_2$- or $HgCl_2$-induced accumulation of phosphorylated JNK in wild-type ES cells. Wild-type ES cells were incubated with 0 μM, 1 μM, 5 μM, 10 μM, 20 μM, or 40 μM $CdCl_2$ (A) or $HgCl_2$ (B) for 1 h. In the time course study, cells were incubated with 20 μM $CdCl_2$ (C) or $HgCl_2$ (D) for 5–60 min. The untreated control is 0 min. Cell lysates were subjected to immunoblotting using anti-phospho-JNK and anti-JNK antibodies. Results shown are representative of three independent experiments.

3. Results

3.1. $CdCl_2$- or $HgCl_2$-induced accumulation of phosphorylated JNK in wild-type ES cells

When wild-type ES cells were incubated with 5 μM of $CdCl_2$ or 20 μM of $HgCl_2$ for 1 h, phosphorylation of JNK (p46 and p54) was found, and the levels of phosphorylated form of JNK increased in a concentration-dependent manner (Fig. 1A and B). In contrast, the levels of total (phosphorylation state-independent) JNK were not changed by incubation with any concentration of $CdCl_2$ or $HgCl_2$. In the time course study, the levels of phosphorylated JNK increased after 30 min or 45 min in response to 20 μM $CdCl_2$ or $HgCl_2$ exposure, whereas total JNK levels were not changed (Fig. 1C and D). Thereafter, ES cells were exposed to $CdCl_2$ or $HgCl_2$ for 1 h at a concentration of 20 μM.

3.2. Suppression of $CdCl_2$- or $HgCl_2$-induced JNK activation in $mkk4^{-/-}$ and $mkk7^{-/-}$ ES cells

As shown in Fig. 2, MKK4 and MKK7 proteins were not detected in $mkk4^{-/-}$ and $mkk7^{-/-}$ ES cells, respectively. Neither MKK4 expression in wild-type and $mkk7^{-/-}$ ES cells nor MKK7 expression in wild-type and $mkk4^{-/-}$ ES cells was affected by the treatment with $CdCl_2$ or $HgCl_2$. In $mkk4^{-/-}$ ES cells, $CdCl_2$- or $HgCl_2$-induced phosphorylation of JNK was abolished almost completely without changing JNK levels (Fig. 3A, lanes 5 and 6). While toxic metal-induced JNK phosphorylation in $mkk7^{-/-}$ ES cells was also reduced significantly, JNK phosphorylation in $mkk7^{-/-}$ ES cells treated with $CdCl_2$ and $HgCl_2$ was 55% and 33% of that in wild-type ES cells treated, respectively (Fig. 3A, lanes 8 and 9). These findings were reproducible with two different anti-phospho-JNK antibodies used in the present study. In contrast to JNK, substantial phosphorylation of other members of MAPK family, p38 and extracellular signal-regulated protein kinase (ERK2/p42 and ERK1/p44), were observed in both, $mkk4^{-/-}$ and $mkk7^{-/-}$ ES cells treated with $CdCl_2$ or $HgCl_2$ (Fig. 3B and C, lanes 5, 6, 8 and 9).

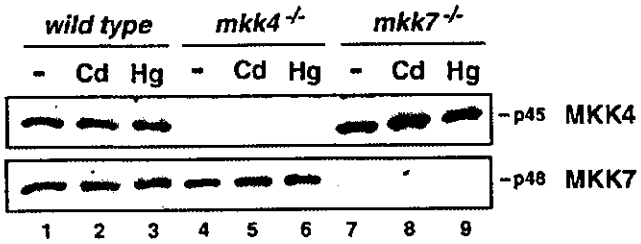

Fig. 2. Effects of $CdCl_2$ or $HgCl_2$ treatment on the levels of MKK4 and MKK7 in wild-type, $mkk4^{-/-}$ and $mkk7^{-/-}$ ES cells. Wild-type, $mkk4^{-/-}$ and $mkk7^{-/-}$ ES cells were incubated with serum-free medium (lanes 1, 4, and 7), 20 μM $CdCl_2$ (lanes 2, 5, and 8) or 20 μM $HgCl_2$ (lanes 3, 6, and 9) for 1 h, and cell lysates were subjected to immunoblotting using anti-MKK4 and anti-MKK7 antibodies. Results shown are representative immunoblot of three independent experiments.

The in vitro activity of JNK assayed using GST-c-Jun as substrate was also examined. Treatment with $CdCl_2$ or $HgCl_2$ induced the marked elevation of JNK activity in wild-type ES cells (Fig. 4, lanes 2 and 3). Consistent with the reduction of phosphorylated JNK levels (Fig. 3A), $CdCl_2$- or $HgCl_2$-induced JNK activation was suppressed in both $mkk4^{-/-}$ and $mkk7^{-/-}$ ES cells. JNK activity in $mkk4^{-/-}$ ES cells treated with $CdCl_2$ and $HgCl_2$ was 12% and 11% of that in wild-type ES cells treated, respectively (Fig. 4, lanes 5 and 6). JNK activity in $mkk7^{-/-}$ ES cells treated with $CdCl_2$ and $HgCl_2$ was 44% and 22% of that in wild-type ES cells treated, respectively (Fig. 4, lanes 8 and 9). Determination of JNK activity based on [$\gamma - {}^{32}P$] incorporation into GST-c-Jun also showed the significant reduction of $CdCl_2$-induced JNK activation in both, $mkk4^{-/-}$ and $mkk7^{-/-}$ ES cells (Nakagawa et al., unpublished data).

4. Discussion

The present study showed that treatment with $CdCl_2$ or $HgCl_2$ induced the accumulation of phosphorylated form of JNK in a dose- and time-dependent manner in wild-type ES cells as has been observed in the various cell types (Matsuoka and Igisu, 2002). In both, $mkk4^{-/-}$ and $mkk7^{-/-}$ ES cells which lack an upstream JNK activator, $CdCl_2$- or $HgCl_2$-induced phosphorylation and activation of JNK were suppressed dramatically. However, in $mkk7^{-/-}$ ES cells treated with $CdCl_2$ and $HgCl_2$, JNK activation was not abolished (suppressed by 56% and 78%, respectively). On the other hand, significant phosphorylation of other members of MAPK, p38 and ERK, was retained in

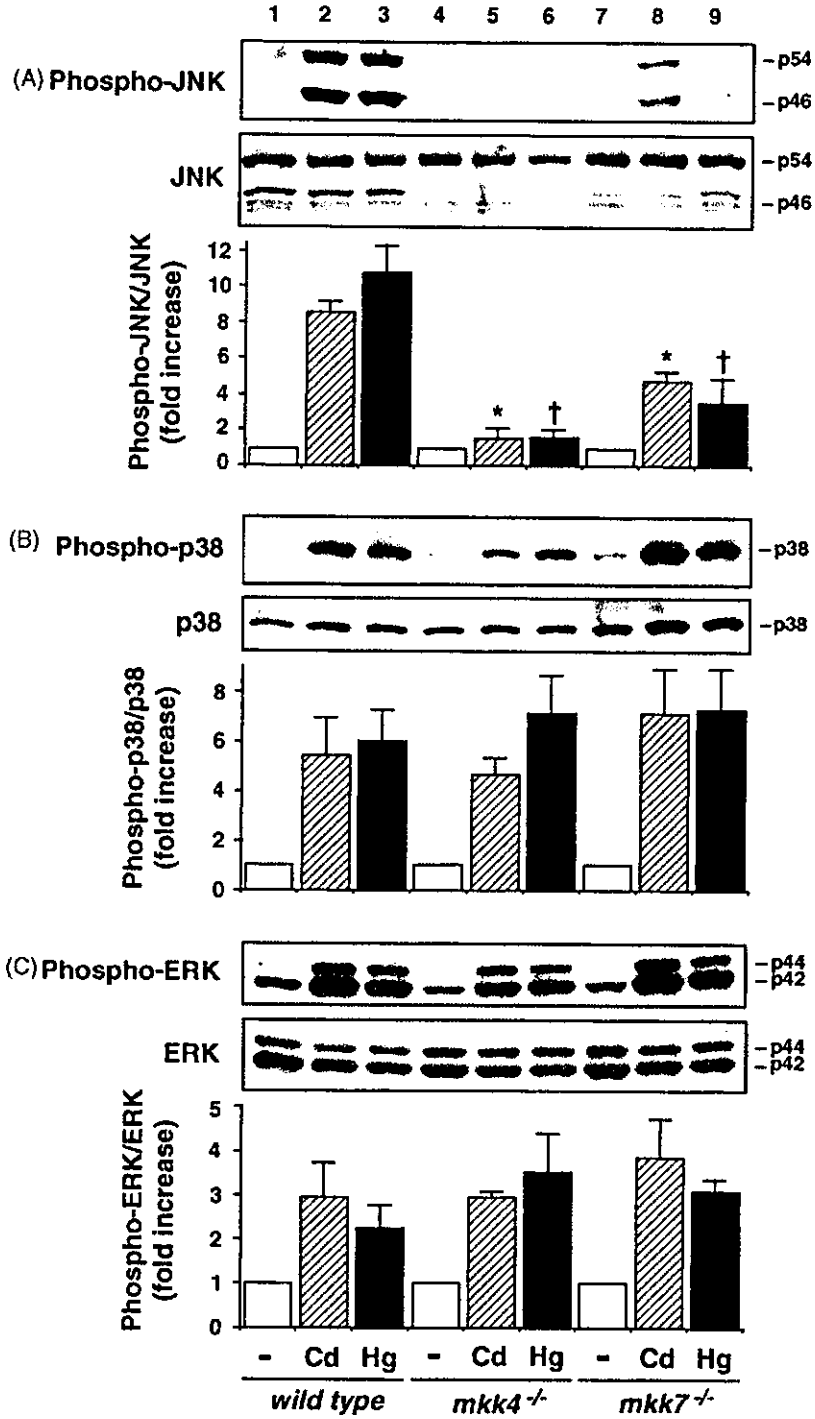

Fig. 3. Effects of $CdCl_2$ or $HgCl_2$ treatment on the levels of phosphorylated JNK (A), phosphorylated p38 (B), and phosphorylated ERK (C). Wild-type, *mkk4*$^{-/-}$ and *mkk7*$^{-/-}$ ES cells were incubated with serum-free medium (lanes 1, 4, and 7), 20 μM $CdCl_2$ (lanes 2, 5, and 8) or 20 μM $HgCl_2$ (lanes 3, 6, and 9) for 1 h, and cell lysates were subjected to immunoblotting using anti-phospho-JNK and anti-JNK antibodies (A), anti-phospho-p38 and anti-p38 antibodies (B), and anti-phospho-ERK and anti-ERK antibodies (C). Results shown are representative immunoblot and densitometric analysis of phosphorylated JNK, p38 and ERK. Each value was expressed as the ratio of phosphorylated MAPK level to the corresponding total MAPK level, and the value of control (without metal treatments) was set to one. Each column and bar represent the mean ± S.D. of three independent experiments. $^{*}P < 0.01$ compared to wild-type ES cells treated with $CdCl_2$, $^{\dagger}P < 0.01$ compared to wild-type ES cells treated with $HgCl_2$.

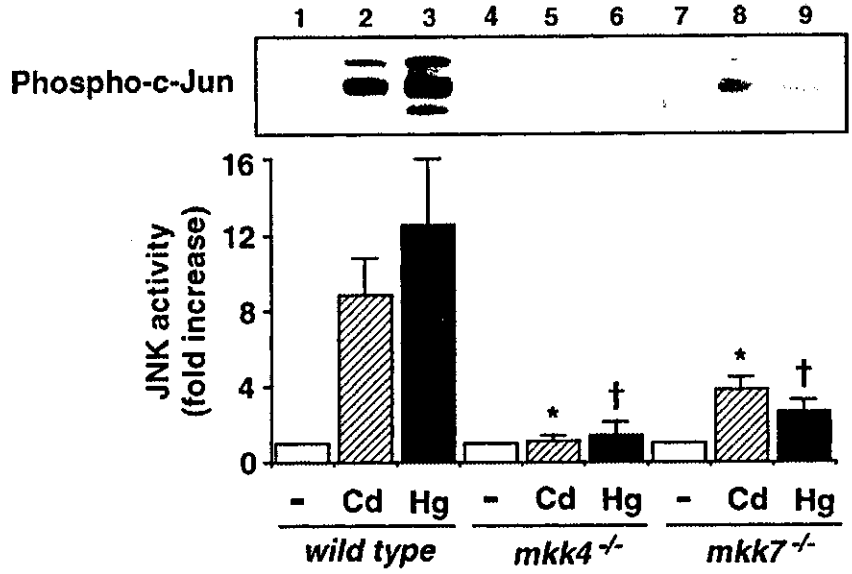

Fig. 4. Effects of $CdCl_2$ or $HgCl_2$ treatment on the activity of JNK in wild-type, *mkk4*$^{-/-}$ and *mkk7*$^{-/-}$ ES cells. Wild-type, *mkk4*$^{-/-}$ and *mkk7*$^{-/-}$ ES cells were incubated with serum-free medium (lanes 1, 4, and 7), 20 μM $CdCl_2$ (lanes 2, 5, and 8) or 20 μM $HgCl_2$ (lanes 3, 6, and 9) for 1 h, and cell lysates were used for in vitro kinase reaction with GST-c-Jun (1–89) as substrate. Phosphorylation of GST-c-Jun was analyzed with immunoblotting using anti-phospho-c-Jun antibody. Results shown are representative immunoblot and densitometric analysis of phosphorylated c-Jun. Each value was expressed as the fold increase with respect to the corresponding control (without metal treatments). Each column and bar represent the mean ± S.D. of four independent experiments. $^{*}P < 0.01$ compared to wild-type ES cells treated with $CdCl_2$, $^{\dagger}P < 0.01$ compared to wild-type ES cells treated with $HgCl_2$.

these mutated cell lines. These findings suggest that the full activation of JNK by toxic metal exposure requires both MKK4 and MKK7, and these upstream kinases might contribute differentially in JNK activation between ES cells exposed to $CdCl_2$ and $HgCl_2$. $CdCl_2$-induced JNK activation seems to depend on MKK4 more extensively than MKK7.

In contrast, previous studies using cells transfected with dominant-negative form of MKK4 or MKK7 showed that cadmium might activate JNK through MKK7, but not MKK4. Transfection with MKK4 mutant elevated $CdCl_2$ (80 μM, 3 h exposure) -induced JNK activation 1.9-fold in human non-small-cell lung carcinoma cells, while expression of MKK7 mutant reduced JNK activity by 35% (Chuang and Yang, 2001). However, expression of MKK7 mutant failed to suppress JNK activity in the same cells treated with a higher concentration of $CdCl_2$ (130 μM) (Chuang et al., 2000). In rat mesangial cells, $CdCl_2$ (10 μM, 8 h exposure) -induced JNK activation was suppressed by 53% when transfected with MKK7 mutant, but not changed by expression of MKK4 mutant (Ding and Templeton, 2000). On the other hand, it has been reported that treatment with $CdCl_2$ induced the phosphorylation of MKK4 in Rat-1 fibroblasts (Iordanov and Magun, 1999), and we also found the phosphorylation of MKK4 on Thr^{261} in wild-type ES cells following exposure to $CdCl_2$ or $HgCl_2$ (data not shown). Thus, MKK4 could be activated by upstream kinase (i.e., MAPK kinase kinase) in response to $CdCl_2$ or $HgCl_2$ exposure, and disruption of the *mkk4* gene abolished toxic metal-induced JNK activation almost completely in ES cells. While the precise functions of MKK4 and MKK7 in cells exposed to toxic metal are still not clear, these MAPK kinases might play a different role in JNK activation depending on the cell type and the experimental condition of exposure. With respect to mkk4$^{-/-}$ and *mkk7*$^{-/-}$ ES cells exposed to $CdCl_2$ or $HgCl_2$, the roles of splice variants and the effects of JNK (p46) expression remain to be examined.

In summary, as has been shown in various stress-induced JNK activation (Kishimoto et al., 2003; Wada et al., 2001), both MKK4 and MKK7 were required for the full activation of JNK in mouse ES cells exposed to $CdCl_2$ or $HgCl_2$. The *mkk4*$^{-/-}$ and *mkk7*$^{-/-}$ ES cells seem to be useful to analyze functions and signaling pathway of JNK activation induced by environmental stresses including toxic metals.

Acknowledgements

We thank Takeo Okuno for technical help. This work was supported in part by Grant-in-Aid for Scientific Research (KAKENHI: 14570313 and 14570315) from the Ministry of Education, Culture, Sports, Science and Technology (MEXT), Japan.

References

Chang, L., Karin, M., 2001. Mammalian MAP kinase signalling cascades. Nature 410, 37–40.

Chuang, S.-M., Yang, J.-L., 2001. Comparison of roles of three mitogen-activated protein kinases induced by chromium (VI) and cadmium in non-small-cell lung carcinoma cells. Mol. Cell. Biochem. 222, 85–95.

Chuang, S.-M., Wang, I.-C., Yang, J.-L., 2000. Roles of JNK, p38 and ERK mitogen-activated protein kinases in the growth inhibition and apoptosis induced by cadmium. Carcinogenesis 21, 1423–1432.

Cobb, M.H., Goldsmith, E.J., 1995. How MAP kinases are regulated. J. Biol. Chem. 270, 14843–14846.

Ding, W., Templeton, D.M., 2000. Stress-activated protein kinase-dependent induction of c-*fos* by Cd^{2+} is mediated by MKK7. Biochem. Biophys. Res. Commun. 273, 718–722.

Iordanov, M.S., Magun, B.E., 1999. Different mechanisms of c-Jun NH_2-terminal kinase-1 (JNK1) activation by ultraviolet-B radiation and by oxidative stressors. J. Biol. Chem. 274, 25801–25806.

Kishimoto, H., Nakagawa, K., Watanabe, T., Kitagawa, D., Momose, H., Seo, J., Nishitai, G., Shimizu, N., Ohata, S., Tanemura, S., Asaka, S., Goto, T., Fukushi, H., Yoshida, H., Suzuki, A., Sasaki, T., Wada, T., Penninger, J.M., Nishina, H., Katada, T., 2003. Different properties of SEK1 and MKK7 in dual phosphorylation of stress-induced activated protein kinase SAPK/JNK in embryonic stem cells. J. Biol. Chem. 278, 16595–16601.

Kyriakis, J.M., Avruch, J., 1996. Sounding the alarm: protein kinase cascades activated by stress and inflammation. J. Biol. Chem. 271, 24313–24316.

Lawler, S., Fleming, Y., Goedert, M., Cohen, P., 1998. Synergistic activation of SAPK1/JNK1 by two MAP kinase kinases in vitro. Curr. Biol. 8, 1387–1390.

Matsuoka, M., Igisu, H., 1998. Activation of c-Jun NH_2-terminal kinase (JNK/SAPK) in $LLC\text{-}PK_1$ cells by cadmium. Biochem. Biophys. Res. Commun. 251, 527–532.

Matsuoka, M., Igisu, H., 2002. Effects of heavy metals on mitogen-activated protein kinase pathways. Environ. Health Prev. Med. 6, 210–217.

Matsuoka, M., Wispriyono, B., Iryo, Y., Igisu, H., 2000. Mercury chloride activates c-Jun N-terminal kinase and induces c-*jun* expression in $LLC\text{-}PK_1$ cells. Toxicol. Sci. 53, 361–368.

Nishina, H., Fischer, K.D., Radvanyi, L., Shahinian, A., Hakem, R., Rubie, E.A., Bernstein, A., Mak, T.W., Woodgett, J.R., Penninger, J.M., 1997. Stress-signalling kinase Sek1 protects thymocytes from apoptosis mediated by CD95 and CD3. Nature 385, 350–353.

Robinson, M.J., Cobb, M.H., 1997. Mitogen-activated protein kinase pathways. Curr. Opin. Cell Biol. 9, 180–186.

Wada, T., Nakagawa, K., Watanabe, T., Nishitai, G., Seo, J., Kishimoto, H., Kitagawa, D., Sasaki, T., Penninger, J.M., Nishina, H., Katada, T., 2001. Impaired synergistic activation of stress-activated protein kinase SAPK/JNK in mouse embryonic stem cells lacking SEK1/MKK4: different contribution of SEK2/MKK7 isoforms to the synergistic activation. J. Biol. Chem. 276, 30892–30897.

Weston, C.R., Davis, R.J., 2002. The JNK signal transduction pathway. Curr. Opin. Genet. Dev. 12, 14–21.

Yu, Z., Matsuoka, M., Wispriyono, B., Iryo, Y., Igisu, H., 2000. Activation of mitogen-activated protein kinases by tributyltin in CCRF-CEM cells: role of intracellular Ca^{2+}. Toxicol. Appl. Pharmacol. 168, 200–207.

ELSEVIER

Mechanisms of Development 121 (2004) 673–685

www.elsevier.com/locate/modo

Research paper

Genetic dissection of the formation of the forebrain in Medaka, *Oryzias latipes*

Daiju Kitagawa[a], Tomomi Watanabe[a], Kota Saito[a], Satoshi Asaka[a], Takao Sasado[b], Chikako Morinaga[b], Hiroshi Suwa[b], Katsutoshi Niwa[b], Akihito Yasuoka[c], Tomonori Deguchi[d], Hiroki Yoda[d], Yukihiro Hirose[e], Thorsten Henrich[b], Norimasa Iwanami[f], Sanae Kunimatsu[f], Masakazu Osakada[g], Chritoph Winkler[h], Harun Elmasri[h], Joachim Wittbrodt[i], Felix Loosli[i], Rebecca Quiring[i], Matthias Carl[i], Clemens Grabher[i], Sylke Winkler[i], Filippo Del Bene[i], Akihiro Momoi[d], Toshiaki Katada[a], Hiroshi Nishina[a], Hisato Kondoh[b,d], Makoto Furutani-Seiki[b,*]

[a]*Department of Physiological Chemistry, Graduate School of Pharmaceutical Sciences, The University of Tokyo, Tokyo 113-0033, Japan*
[b]*Japan Science and Technology Agency, ERATO, Kondoh Differentiation Signaling Project, Kawaracho14, Yoshida, Sakyoku, Kyoto 606-8305, Japan*
[c]*Graduate School of Agricultural and Life Sciences, The University of Tokyo, Tokyo 113-0033, Japan*
[d]*Graduate School of Frontier Biosciences, Osaka University, Osaka, 565-0871, Japan*
[e]*Graduate School of Biostudies, Kyoto University, Kyoto 606-8502, Japan*
[f]*Division of Experimental Immunology, Institute for Genome Research, The University of Tokushima, Tokushima 770-8503, Japan*
[g]*Department of Molecular Medicine and Pathophysiology, Research Institute, Osaka Medical Center for Cancer and Cardiovascular Diseases, Osaka 537-8511, Japan*
[h]*Department of Physiological Chemistry I, Biocenter, University of Wuerzburg, Wuerzburg, Germany*
[i]*Developmental Biology Programme, EMBL, D-69117, Heidelberg, Germany*

Received 1 February 2004; received in revised form 16 March 2004; accepted 18 March 2004

Abstract

The forebrain, consisting of the telencephalon and diencephalon, is essential for processing sensory information. To genetically dissect formation of the forebrain in vertebrates, we carried out a systematic screen for mutations affecting morphogenesis of the forebrain in Medaka. Thirty-three mutations defining 25 genes affecting the morphological development of the forebrain were grouped into two classes. Class 1 mutants commonly showing a decrease in forebrain size, were further divided into subclasses 1A to 1D. Class 1A mutation (1 gene) caused an early defect evidenced by the lack of *bf1* expression, Class 1B mutations (6 genes) patterning defects revealed by the aberrant expression of regional marker genes, Class 1C mutation (1 gene) a defect in a later stage, and Class 1D (3 genes) a midline defect analogous to the zebrafish *one-eyed pinhead* mutation. Class 2 mutations caused morphological abnormalities in the forebrain without considerably affecting its size, Class 2A mutations (6 genes) caused abnormalities in the development of the ventricle, Class 2B mutations (2 genes) severely affected the anterior commissure, and Class 2C (6 genes) mutations resulted in a unique forebrain morphology. Many of these mutants showed the compromised *sonic hedgehog* expression in the zona-limitans-intrathalamica (zli), arguing for the importance of this structure as a secondary signaling center. These mutants should provide important clues to the elucidation of the molecular mechanisms underlying forebrain development, and shed new light on phylogenically conserved and divergent functions in the developmental process.

Keywords: Forebrain; Telencephalon; Diencephalon; Mutants; Medaka; Mutagenesis screen

1. Introduction

The vertebrate forebrain, consisting of the telencephalon and diencephalon, is formed at the most rostral portion of the developing central nervous system (CNS). The telencephalon is the highest-order processor of neural functions,

* Corresponding author. Tel./fax: +81-75-771-9362.
E-mail address: furutaniseiki@msi.biglobe.ne.jp (M. Furutani-Seiki).

0925-4773/$ - see front matter © 2004 Elsevier Ireland Ltd. All rights reserved.
doi:10.1016/j.mod.2004.03.010

and the diencephalon is the conduit for ascending sensory information. Each territory of the forebrain is further regionalized along the respective anteroposterior (AP) and dorsoventral (DV) axes. These structures in the forebrain and their connections are essential for processing sensory information, integrating of new sensory information with established memories, and then formulating and effecting behavioral responses (Wilson and Rubenstein, 2000; Rallu et al., 2002).

The vertebrate forebrain was proposed to be subdivided in a segment-like manner into transverse neuromeric domains (prosomeres) analogous to rhombomeres in the hindbrain; on the basis of restricted expression patterns of transcription factors (neuromeric model, Bulfone et al., 1993; Figdor and Stern, 1993; Puelles and Rubenstein, 1993; Hauptmann and Gerster, 2000).

In all vertebrates, the developing telencephalon is subdivided into the dorsal (pallial region, expressing *emx1*) and ventral (subpallial region, expressing *dlx2*) domains. In the mammalian telencephalon, dorsal, pallial regions give rise to the cortex, while ventral, subpallial regions give rise to the basal ganglia. Similar pallial and subpallial subdivisions of the telencephalon exist in all vertebrates (Fernandez et al., 1998; Puelles et al., 2000), although the adult derivatives of these subdivisions vary among species.

The diencephalon is proposed to be divided into four longitudinal neuronal zones—dorsally, epithalamus, dorsal thalamus, ventral thalamus; and ventrally, hypothalamus (Figdor and Stern, 1993; Hauptmann et al., 2002). The dorsal and ventral thalami are divided by the zona limitans intrathalamica (zli). Although it is yet to be proven, the zli has been suggested to be a secondary signaling center, since the secreted signaling protein *sonic hedgehog* (*shh*) is expressed in the zli.

Theories of the formation of the subdivisions of the forebrain, however, are established on the bases of restricted expression patterns, mostly of transcription factors. Most of these transcription factors were cloned either by the homology of genes identified in the forward genetic mutant screening of invertebrates, such as *Drosophila melanogaster* and *Caenorhabditis elegans*, or by expression pattern screening. Functional studies of these genes have been carried out by the reverse genetic approach in the mouse or gain-of-function studies in chick, *Xenopus* and zebrafish. These studies, however, were still limited to the genes initially cloned by homology or expression patterns, but not their functions.

Genome-wide forward genetic screening based on the functions of genes, carried out using zebrafish for the first time in vertebrates, together with gene knock-out mice, established a genetic basis for the three key signaling pathways for the patterning of the forebrain. The Nodal pathway acts upstream of Shh signaling to specify the ventral telencephalon (Rohr et al., 2001; Varga et al., 2001), but Nodal and Shh signaling have distinct and cooperative roles in the development of the ventral diencephalon (Mathieu et al., 2002). However, the precise roles of Shh signaling, such as the source and time of action for the patterning the forebrain, remain to be elucidated. Wnt signaling is also reported to be important for patterning of the forebrain along the anteroposterior (A–P) axis (Kim et al., 2000; Heisenberg et al., 2001). The first row of cells at the rostral margin of the neural plate were shown to pattern the anterior forebrain anteroposteriorly (Houart et al., 1998) and its function has been ascribed to the secretion of the Wnt antagonist, *tlc* (Houart et al., 2002), corroborating the importance of Wnt signaling for A–P patterning in the forebrain in zebrafish. Nevertheless, insights obtained from existing mutants are still fragmentary due to the limited number of mutants.

In vertebrates in which the functions of multiple genes often overlap, mutagenesis screens in a single species is not sufficient for uncovering all functioning genes in a genetic cascade or in the development of an organ, but this limitation should be largely alleviated by the use of another related animal species. Thus, to define the genetic components of the signaling required for patterning of the forebrain and their interplay, we have undertaken a large-scale mutagenesis screen in Medaka. Here, we report the initial characterization of 33 mutations in 25 complementation groups exhibiting specific defects in the development of the forebrain. These mutants show a reduction in the size of the telencephalon, and defects in the formation of the ventricle or axogenesis. These mutants are often phenotypically distinct from those of mutants isolated in zebrafish (Brand et al., 1996a,b; Furutani-Seiki et al., 1996; Heisenberg et al., 1996; Schier et al., 1996), supporting the importance of this fish species which complements zebrafish.

2. Results

2.1. Development and regionalization of forebrain in wild-type Medaka embryos

The forebrain formed at the most rostral portion of the neural plate is composed of the telencephalon and diencephalon, occupying its dorsoanterior and ventroposterior portions, respectively. In Medaka, the forebrain becomes distinguishable from the midbrain at the histological level at stage 19 (st. 19), 27 hours post fertilization (hpf) at 28 °C (Fig. 1A), (Iwamatsu, 1994), and morphologically at st. 21 (Fig. 1B). During st. 19 and 21, the tissue initially located at the rostral end of the brain tissue is displaced to the ventral side of the brain. At st. 23 (41 hpf), the forebrain ventricle starts to form (Fig. 1C). During st. 23 and st. 27, the initially linear anteroposterior (A–P) axis through the brain is bent in the diencephalon area forming the ventral diencephalon (hypothalamus) overlain by both the dorsal diencephalon and mesensephalon, thereby

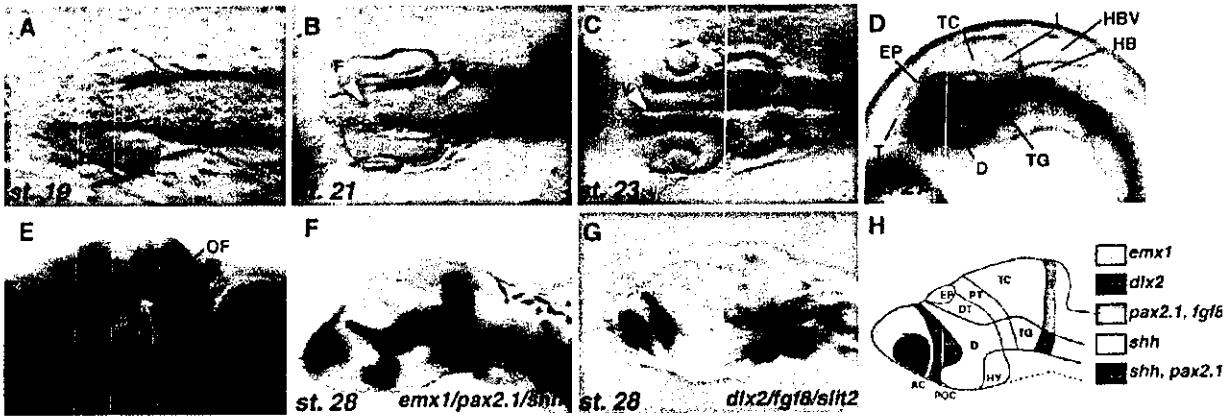

Fig. 1. Development and regionalization of the forebrain in wild-type Medaka embryos. (A–D) Morphology of the brain in Medaka live embryos. Dorsal view of wild-type embryo at (A) st. 19, (B) st. 21, (C) st. 23, (D) lateral view of the embryo at st. 27. (E) Major axonal scaffolds in the forebrain. Whole-mount immunostaining with anti-acetylated-tubulin and anti-HNK antibodies at st. 31. Ventral view of anterior portion of the head. (F,G) Whole-mount in situ hybridization analysis at st. 28. (F) *emx1*, *pax2.1*, *shh*; and (G) *dlx2*, *fgf8*, *slit2* as probes. (H) Schematic representation of gene expression patterns in subdivisions of the forebrain and midbrain. AC, anterior commissure; D, diencephalon; DT, dorsal thalamus; EP, epiphysis; F, forebrain; FV, forebrain ventricle; HB, hindbrain; HBV, hindbrain ventricle; HY, hypothalamus; I, isthmus; M, midbrain; OF, olfactory nerve; ON, optic nerve; POC, post-optic commissure; PT, pretectum; SOT, supraoptic tract; T, telencephalon; TC, tectum; TG, tegmentum; VT, ventral thalamus.

establishing the dorsoventral axis of the diencephalon (Fig. 1D). The cell layer of the roof of the telencephalon loses their thickness, and the telencephalon assumes its characteristic morphology. During st. 28–34 (64–131 hpf), cells proliferate extensively in the ventricular zone, and the ventricle loses its space (Ishikawa and Hyodo-Taguchi, 1994). The major axonal scaffolds in the forebrain, including commissural neurons, the supraoptic tract and sensory nerves, are formed by st. 34 (Fig. 1E).

In zebrafish, it was demonstrated that the expression patterns of marker genes define the transverse and longitudinal subdivisions within the forebrain and midbrain (Macdonald et al., 1994; Hauptmann and Gerster, 2000). Expression patterns of these markers seem to be well conserved in Medaka (Fig. 1F–H). For the initial characterization of Medaka forebrain mutants, we carried out whole-mount in situ hybridization analysis using a mixture of probes, *emx1/pax2.1/shh* and *dlx2/fgf8/slit2*. The dorsal and ventral telencephalon express *emx1* and *dlx2*, respectively. The diencephalon is divided into four domains; dorsal and ventral thalami, pretectum and hypothalamus. The zona limitans intrathalamica (zli), which expresses *shh*, divides the dorsal and ventral thalami. The ventral thalamus is marked by *dlx2* expression.

2.2. Identification of forebrain mutants in Medaka

Since a specific patterning defect often causes later occurrence of localized cell degeneration (Furutani-Seiki et al., 1996), we paid special attention to morphological abnormalities accompanied by cell degeneration. In the large-scale mutagenesis screen for embryonic pattern formation, we identified 33 mutations affecting forebrain development in Medaka mutants, exhibiting a variety of morphological defects and/or abnormal axonal pathways. These mutations were assigned to 25 complementation groups (Table 1). We classified these mutations into two groups, on the basis of the type of defects in the telencephalon. Class 1 mutations were those primarily affecting the size of the telencephalon, while Class 2 mutations were those mainly causing abnormalities in the forebrain shape without significantly affecting the size of the telencephalon. All the isolated mutations were zygotic recessive, and in this paper homozygous embryos are referred to as mutants. Two mutations turned out to be temperature sensitive; $kar^{j50\text{-}4A}$, which is sensitive to a low temperature (18 °C); and $ika^{j94\text{-}8A}$, which is sensitive to a high temperature (33 °C).

2.3. Class 1 mutations affecting telencephalon size

We have identified 15 mutations in 11 genes of this class causing reduction in telencephalon size (Fig. 2, arrowheads in A–F). According to the onset of the phenotype, we classified the Class 1 mutations into four subclasses, as summarized in Table 1.

2.3.1. Class 1A and 1B mutations affecting subregions of the telencephalon

In *kentoku* ($ket^{j23\text{-}3B}$) and *aonibi* ($aon^{j9\text{-}2F}$) mutant embryos, morphological defects appeared to be restricted to the telencephalon (Fig. 2B,C), whereas in *kobesshimi* ($kob^{j35\text{-}6D}$) and *bouzu* ($bou^{jr118\text{-}2A}$) mutant embryos, size reduction occurred also in the midbrain (Fig. 2D,E). On the other hand, *nopperabo* ($nop^{j80\text{-}19B}$) mutant embryos exhibited a characteristic phenotype, that is a reduction in forebrain size accompanied by the enlargement of the midbrain, reminiscent of that of *masterblind* (*mbl*) and *headless* (*hdl*) mutants in zebrafish (Fig. 2F).

Class 1 mutant embryos at st. 31 were immunochemically stained with anti-acetylated-tubulin and HNK1

Table 1
Mutations affecting formation of the forebrain

Gene	Symbol	Alleles	Forebrain phenotype	Other phenotypes
Class 1: mutations affecting the size of the telencephalon				
Class 1A: mutations affecting early specification of the telencephalon				
kentoku	*ket*	*j23-3B*	Telencephalon size reduced	
Class 1B: mutations affecting regionalization of the telencephalon				
aonibi	*aon*	*j9-2F, j60-3A*	Telencephalon size reduced	Lipid metabolism affected
kobesshimi	*kob*	*j9-10A, j35-6D, j54-3A*	Telencephalon size reduced	Midbrain slightly reduced
bouzu	*bou*	*jr118-2A*	Telencephalon size reduced	Midbrain anteroposteriorly reduced
nopperabo	*nop*	*j80-19B*	Telencephalon size reduced	Eyes missing, midbrain expanded
kumasaka	*kum*	*j54-20A*	Telencephalon size reduced	
usobuki	*uso*	*j14-26A*	Telencephalon size reduced	
Class 1C: a mutation affecting maintenance of the telencephalon				
hannya	*han*	*j41-3B*	Late telencephalon defect	–
Class 1D: mutations affecting formation of the midline neural tissue				
akatsuki	*aku*	*j22-15A, jf121-1A*	Telencephalon size reduced	Similar to zebrafish *oep*
akebono	*ake*	*j54-7A*	Telencephalon size reduced	Similar to zebrafish *oep*
mochizuki	*moc*	*j96-11B*	Telencephalon size reduced	Similar to zebrafish *oep*
Class 2: mutations affecting morphology of the telencephalon				
Class 2A: mutations affecting formation of the forebrain ventricle				
sarudahiko	*sar*	*j106-4A*	Forebrain ventricle reduced	Circulation, midline defect, tectum reduced
tengu	*ten*	*j2-11A, jr10-4D, j53-4C*	Forebrain ventricle reduced	Circulation, midline defect, tectum reduced
karuna	*kar*	*j50-4A*	Forebrain ventricle enlarged	Temperature sensitive at 18 °C
oobesshimi	*oob*	*j103-11A, j58-1A*	Forebrain ventricle enlarged	Tegmentum and hindbrain bumpy
samidare	*sam*	*j20-26A*	Forebrain ventricle enlarged	Similar to zebrafish *parachute* mutant
shigure	*sgu*	*j55-8A*	Forebrain ventricle enlarged	Similar to zebrafish *parachute* mutant
Class 2B: mutations affecting the formation of the anterior commissure				
ikazuchi	*ika*	*j94-8A*	Ectopic anterior commissure	Temperature sensitive at 33 °C, hindbrain bumpy
shikami	*shi*	*j92-3A*	Anterior commissure not formed	–
Class 2C: mutations causing forebrain dysmorphology				
baltan	*bal*	*j102-2A*	Forebrain dysmorphology, edema	Eyes small, tectum reduced, circulation defect, somite irregular
fukuwarai	*fuk*	*j8-33A, j93-4A*	Forebrain dysmorphology	Regions of CNS misplaced
yuzen	*yuz*	*j107-2D*	Forebrain dysmorphology	Regions of CNS misplaced
kagome	*kag*	*jr114-2D*	Forebrain dysmorphology	Regions of CNS misplaced
hirame	*hir*	*j54-20C*	Flattened, differentiation defect	CNS flat, heart beating next to ears
tobi	*tob*	*jr116-4A*	Protruding telencephalon	Eyes small

antibody to examine the paths and fasciculation of axons (Fig. 2G–L). In the wild type embryos, the olfactory nerve, anterior commissure, supraoptic tract and optic nerve were clearly stained (Fig. 2G). All Class 1 mutants showed interesting abnormalities in these nerves. In *ket* mutant embryos, anterior commissure nerves were not fully fasciculated (black arrowhead in Fig. 2H), displaced and lacked association with the olfactory nerve (white arrowheads in Fig. 2H), and the supraoptic tract was not clearly detected. In *aon* mutant embryos, the olfactory nerve and supraoptic tract were not detected, the anterior commissure lacked fasciculation (white arrowhead in Fig. 2I), and bundle formation of the optic nerve was also affected (black arrowhead in Fig. 2I). *kob* mutants were unique in that only olfactory nerve was affected and lacked fasciculation (arrowhead in Fig. 2J). In *bou* mutant embryos, the axons in the anterior commisure were totally defasciculated, and the commissure did not form (arrowhead in Fig. 2K). In the *nop* mutant embryos, all axonal paths were so severely affected and in astray that the nerves in the forebrain were not morphologically distinguishable each other (arrowhead in Fig. 2L). In addition, the olfactory bulbs appeared to be missing in *nop* mutant embryos (Fig. 2L). Thus, Class 1 mutants share the commonality of a reduced telencephalon size, but alterations of the nerves and their paths were affected distinctly.

Class 1 mutants were also examined for the regional markers of the forebrain by in situ hybridization with two sets of probes, *emx1/pax2.1/shh* and *dlx2/fgf8/slit2* (Fig. 2M–X). Consistent with a smaller telencephalon, Class 1 mutant embryos generally showed a reduction in *emx1* or *dlx2* expression in the telencephalon.

In *ket* and *nop* mutant embryos, the *emx1* expression was strongly reduced (black arrowhead in Fig. 2N,R) and

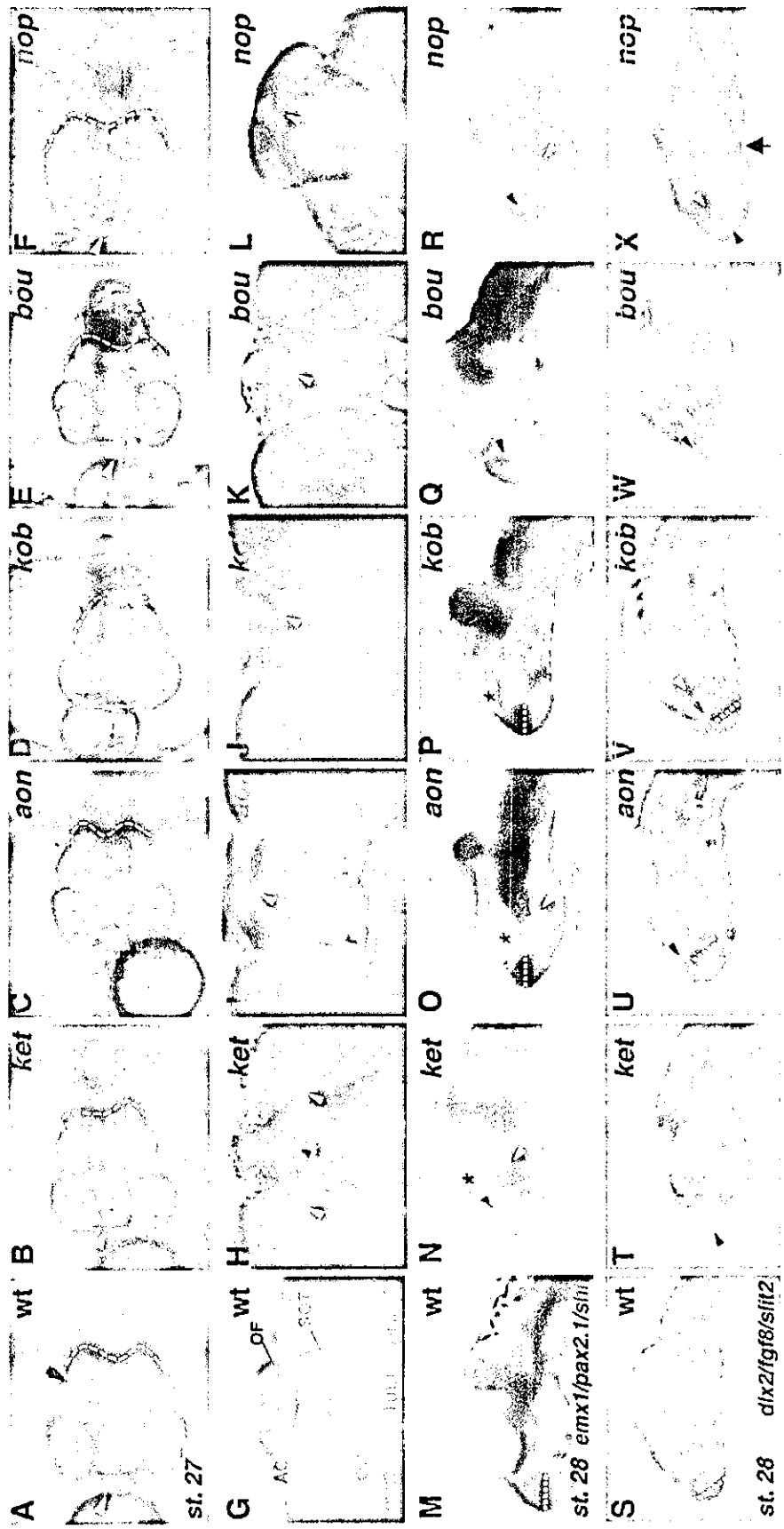

Fig. 2. Class 1 mutant phenotypes. (A,G,M,S) Wild type; (B,H,N,T) $ket^{t23\text{-}3B}$; (C,I,O,U) $aon^{t9\text{-}2F}$; (D,J,P,V) $kob^{t35\text{-}6D}$; (E,K,Q,W) $bou^{t118\text{-}2A}$; (F,L,R,X) $nop^{t80\text{-}19B}$ embryos. (A–F) Phenotypes of live Class 1 mutant embryos at st. 27 (dorsal view). White and black arrowheads indicate the positions of the telencephalon and midbrain, respectively. All Class 1 mutants show a reduction in the size of the telencephalon. Broken lines indicate the posterior edges of the telencephalon and the midbrain. (G–L) Whole-mount immuno-staining with anti-acetylated-tubulin and anti-HNK antibodies of embryos at st. 31. Ventral view of the anterior portion of the head. AC, anterior commissure; SOT, supraoptic tract; OF, olfactory nerve; ON, optic nerve. (M–X) In situ hybridization analysis of the forebrain of embryos at st 28. Lateral view of the head. (M–R) *emx1/pax2.1/shh*, and (S–X) *dlx2/fgf8/slit2* as probes, respectively.